Chatter Maps for Process Design of Powertrain Components

L. Masset, J.-F. Debongnie
Manufacturing Laboratory, ASMA Department, University of Liège, Belgium

W. Belluco
Process Engineering, Renault Powertrain Division, Rueil-Malmaison, France

Abstract
During rough machining operations of powertrain components, chatter vibrations may occur on the edges of flexible structures. This paper presents a numerical method, based on the finite element method and *Tlusty's theory*, which gives a *chatter map* of the machined surface. Each map point represents the greatest depth of cut leading to unconditionally stable cut. Each value depends on the structural damping, the cutting stiffness and the local static stiffness, which is computed using conventional linear elastic FEA. Chatter maps offer a convenient and effective decision support system for *robust process design*. As a case study, the rough milling operation of a crankcase deck face with a two-stage cutter is presented.

1 INTRODUCTION

In the automotive industry, weight reduction is a crucial issue. Process designers for automotive powertrains are increasingly confronted with parts that are optimised (with respect to weight) according to their functional requirement in service life. However, the mass production of such high quality components at low costs may be challenging if no quantitative tools are available to process designers. In particular, the need exists to predict accurately quality parameters (for instance form accuracy). The most efficient method for controlling and improving form accuracy is the integration of the form-accuracy requirements into manufacturing process design *and* product design. The effect of unreliable manufacturing process design may be catastrophic: difficult quality control, excessive manufacturing costs and inadequate production capacity.

Surface errors are generated as a consequence of the relative motion between tool and workpiece. When correct machine tool and workpiece set-up are performed, surface errors are due to the machining process. Common influence factors are theoretical kinematics (for instance tool geometry replica or tool path), geometrical inaccuracy of machine tool and cutting tools (spindle run-out, guide ways straightness and misalignment, tool setting), deformation of the machining system under external forces (cutting, clamping, gravity, inertia), deformation of the machining system under thermal load, deformation of the workpiece by internal stresses and microstructural variations of the material.

A number of studies have been conducted in the area of the prediction of deformations of the machining system under mechanical and thermal loads using finite element analysis.

Shultz [1] presented examples of form error predictions of a crankcase deck face. Stephenson [2] studied examples of crankcase machining in milling and boring. Liu et al [3] studied some effects of mechanical and thermal load during cylinder boring, including some considerations on process dynamics. Kakade and Chow [4] analyzed engine bore distortions.

Subramani et al. [5] developed a model for the prediction of temperature distorsions in bores.

Despite the validity of the finite element analysis under certain manufacturing conditions, most approaches are based on time domain simulations, featuring excessive computational cost for a systematic adoption in industrial product-process design loops.

Masset and Debongnie [6,7] predicted form error induced by workpiece deformation under clamping and cutting loads, using finite element analysis and the superelement method with a *quasi-static approach*; a dramatic reduction of the computational cost was achieved, and the simulation of complex industrial parts was made possible on a common personal computer.

This work is concerned with the implementation of chatter limit prediction in finite element analysis of machining operations using a quasi-static approach.

A number of researchers have clarified the mechanics of machining chatter and stability lobe prediction. (Tlusty, Tobias, Merrit, Altintas, Smith, Davies, ...) and a CIRP keynote paper [8] on machining chatter will be presented at the CIRP General Assembly 2004 by Altintas. In this paper, using Tlusty's theory, we propose chatter maps as a simple and cost-effective decision-support methodology for process design.

2 THEORETICAL BACKGROUND

2.1 Tlusty's Theory

Regenerative chatter occurs because the cutting process is a closed-loop system: vibrations of the system induce a wavy cut surface; the chip thickness variations induce a variable cutting force component that causes additional system vibration.

Let us first recall the well-known Tlusty's theory of regenerative chatter [9]. The dynamic behaviour of the machine tool can be modelled with the single degree of freedom system (SDOF) shown on Figure 1. For a sinusoidal external force, the transfer function (TF) of the system is given by

$$G(\omega) = \frac{X(\omega)}{F(\omega)} = \frac{1}{k}\frac{1}{1-r^2+2j\,\zeta r} \qquad (1)$$

where r is the ratio between the external force frequency ω and the natural frequency of the system ω_0, k is the static stiffness and ζ is the damping ratio.

Direction y is the normal to the cut surface. The vibration motion is inclined from an angle α and the cutting force from an angle β.

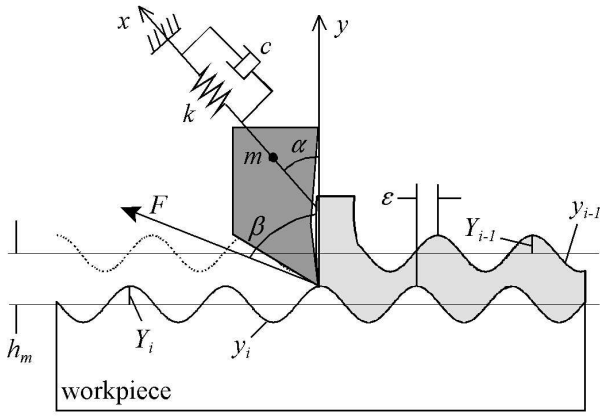

Figure 1: model of regenerative chatter.

The instantaneous chip thickness is the sum of a constant component h_m and a variable one depending on the previous cut y_{i-1} and the current undulation y_i. The regenerative force dF is given by

$$dF = k_d b\,(x_{i-1} - x_i)\cos\alpha \qquad (2)$$

where b is the chip width and k_d is the *cutting stiffness* (increment in the magnitude of the cutting force at unit chip width). The amplitude of vibration is given by eq. (1),

$$x_i = dF\cos(\alpha-\beta)G(\omega) \qquad (3)$$

The ratio between previous and current undulations is given by

$$\frac{y_i}{y_{i-1}} = \frac{x_i}{x_{i-1}} = \frac{uG(\omega)}{uG(\omega)+k_d b} \qquad (4)$$

where u is a directional coefficient accounting the orientation of the cutting force and the orientation of the vibration motion. According to Tlusty, the system is unstable if the vibratory motion increases with time. It is stable if it de-

creases or remains constant. Thus, the limit of stability is obtained for

$$\left|\frac{y_i}{y_{i-1}}\right| = 1 \;\Leftrightarrow\; \left|\frac{x_i}{x_{i-1}}\right| = 1 \tag{5}$$

Equating the magnitude of eq. (4) to unity leads to the stability criteria,

$$b_{cr} = \frac{-1}{2k_d u\,\mathrm{Re}\{G(\omega)\}} \tag{6}$$

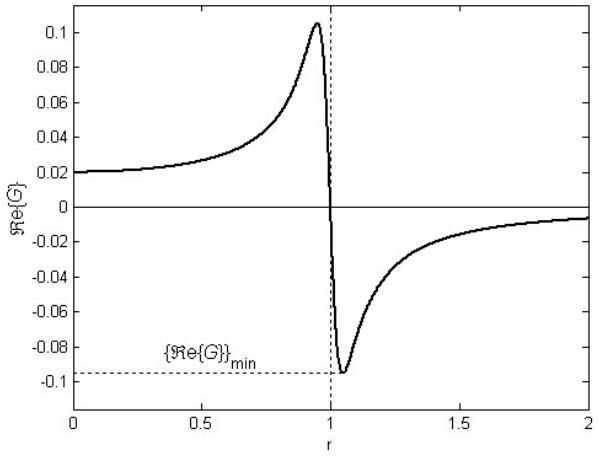

Figure 2: Real part of the TF.

The absolute limit of stability b_{lim} is obtained for the largest negative value of the real part of the TF (Figure 2). Therefore,

$$b_{\lim} = \frac{2k\,\zeta\,(\zeta+1)}{k_d u} \tag{7}$$

The limit value b_{lim} is the greatest width of cut for which no chatter occurs at any frequency. For a multiple degree of freedom system (MDOF), eq. (6) becomes

$$b_{cr} = \frac{-1}{2k_d \sum_i u_i\,\mathrm{Re}\{G_i(\omega)\}} \tag{8}$$

since the TF of a complex system is the sum of the TF of its individual modes.

2.2 Flexibility Maps

The prediction of form error requires the computation of several mechanical deformations of the part/fixture system [6,7]. In order to reduce the computational cost, we use the *superelement method*. All the system degrees of freedom except the ones linked to relevant surfaces of the part (clamping and support zones, machined surface) are condensed (Figure 3).

$$\begin{array}{c|c|c|c} & \boldsymbol{K} & \boldsymbol{q} & \boldsymbol{g} \\ \hline \boldsymbol{K}_{RR} & \boldsymbol{K}_{RC} & \boldsymbol{q}_R & \boldsymbol{g}_R \\ \hline \boldsymbol{K}_{CR} & \boldsymbol{K}_{CC} & \boldsymbol{q}_C & \boldsymbol{0} \end{array}$$

$$\Leftrightarrow \left[\boldsymbol{K}_{RR} - \boldsymbol{K}_{RC}\boldsymbol{K}_{CC}^{-1}\boldsymbol{K}_{CR}\right]\boldsymbol{q}_R = \boldsymbol{g}_R$$

$$\Leftrightarrow \boldsymbol{K}_{RR}^{*}\,\boldsymbol{q}_R = \boldsymbol{g}_R$$

Figure 3: Superelement method.

This way, the system size is reduced, typically by a factor 10 to 100. After having applied the boundary conditions, the reduced stiffness matrix is inverted,

$$\boldsymbol{q}_R = \boldsymbol{K}_{RR}^{*-1}\,\boldsymbol{g}_R \;\Leftrightarrow\; \boldsymbol{q}_R = \boldsymbol{S}\,\boldsymbol{g}_R \tag{9}$$

The matrix $\boldsymbol{S}$ is called the flexibility matrix. Each column represents the displacement field induced by a unit force on the corresponding dof. Each diagonal sub-matrix of dimension 3x3 reflects the direct flexibility of a node while the non-diagonal terms reflect the coupling between nodes (Figure 4).

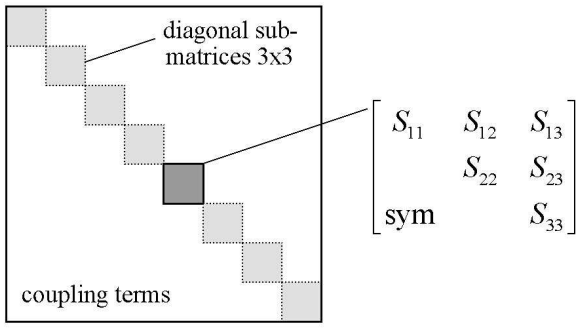

Figure 4: Flexibility matrix.

If we take only the diagonal sub-matrices corresponding to the nodes of the machined surface, we can plot flexibility maps of the machined surface. Figure 5 illustrates the flexibility map of the machined surface of a thin plate. The displayed values are the diagonal terms S_{33} of the flexibility sub-matrices in the third direction (normal to the machined surface).

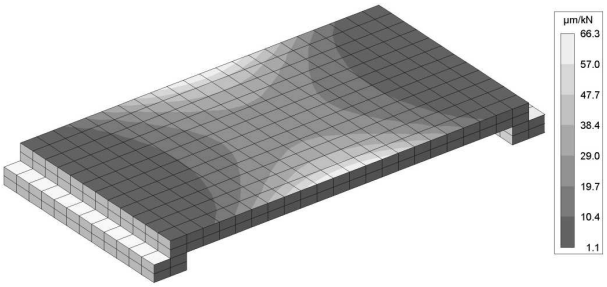

Figure 5: Example of a flexibility map.

3 CHATTER MAPS

3.1 Principle

The stability criterion given by eq. 8 is well suited for simple models such as tools. Such models do not apply for complex parts because the stiffness varies greatly between different zones of the workpiece. The only way to deal with complex parts is to compute the TF of the machined surface thanks to a FE code but this task is time consuming.

The most relevant idea of our method is to combine Tlusty's theory and the flexibility map to obtain a *chatter map* of the machined surface.

$$\boldsymbol{S} = \begin{bmatrix} 8.34 & -0.94 & 0.32 \\ & 80.74 & -26.22 \\ sym & & 18.32 \end{bmatrix} \quad \boldsymbol{s'} = \begin{bmatrix} 90.3 & & \\ & 8.8 & \\ & & 8.3 \end{bmatrix} \quad \begin{cases} \vec{v}_1 = [-0.01 \quad 0.94 \quad -0.34] \\ \vec{v}_2 = [-0.04 \quad 0.34 \quad 0.94] \\ \vec{v}_3 = [\ 0.99 \quad 0.02 \quad 0.03] \end{cases}$$

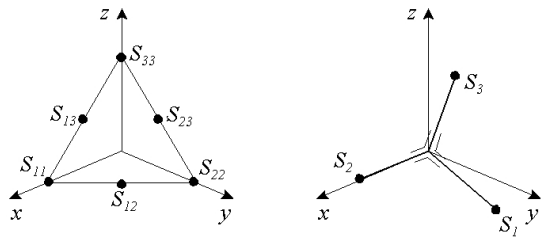

Figure 6: Main flexibility directions and values

Let us consider one node and its corresponding sub-matrix $\boldsymbol{S_{33}}$. The eigenvalues of the sub-matrix are the *main flexibility terms*. Each one corresponds to a main direction given by the associated eigenvector (Figure 6). The eigenvectors are orthogonal because of the symmetry of the flexibility matrix. Thus, we obtain a new sub-matrix with no coupling terms.

We consider that each node of the machined surface is a 3DOF system for which we *should* apply the stability criteria (eq. 8). The problem is that the mass of this virtual system is unknown, so we are unable to compute the natural frequencies and the real part of its TF (Figure 7). To get round the problem, we only take into account the flexibility associated with the first system eigenmode, i.e. the greatest flexibility of the node.

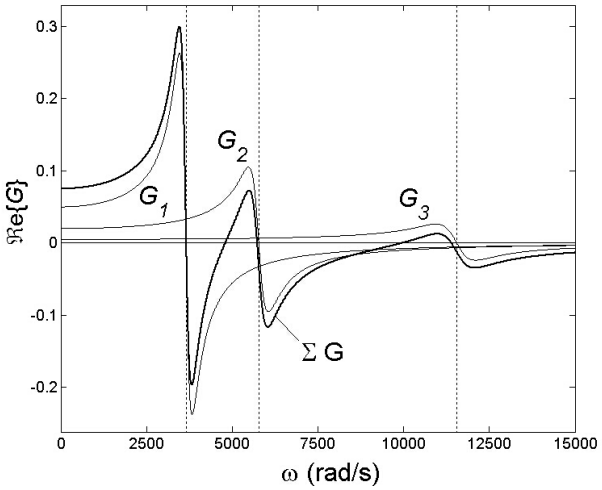

Figure 7: Real part of the TF of a 3DOF system.

This simplification is valid if the modes are clearly separated. In practice, this assumption is true for the zones of the machined surface that are likely to become unstable.

3.2 Computation

To obtain the chatter map, we have to apply the stability criteria for each node of the machined surface. If we get back to eq. 7, we just have to replace the stiffness term k by the inverse of the greatest flexibility,

$$a_{\lim} = \frac{2\zeta(\zeta+1)}{s_1 k_d u}\cos\gamma_L \qquad (10)$$

where $a_{\lim}$ is the depth of cut, γ_L is the tool lead angle and s_1 is the greatest flexibility value. The three terms of the denominator vary from one node to another.

This approach is *solely* valid in the case where *only one insert is engaged on the flexible structure at a time*. Practically, this situation is met for thin walls for which chatter occurs easily.

The damping ratio ζ is supposed to be the same for all the nodes. It should reflect the global system damping: process damping, structural damping and other damping sources such as friction at the contact zone between the part and the fixture devices. In practice, we only take into account the stuctural damping. It can be obtained through modal tests or by taking characteristic properties of material (3 to 6% for cast iron).

The cutting stiffness k_d is obtained from the material cutting properties. Usually, only the main cutting force is known through the Kienzle law,

$$F_c = k_c\, b\, h^{1-m_c} \tag{11}$$

We assume that the ratio A between the repulsion force and the main cutting force is a constant (from 0.4 to 0.6). The cutting stiffness is given by

$$k_d = \sqrt{1+A^2}\;\; k_c(1-m_c)\; h^{-m_c} \tag{12}$$

The direction of the repulsion force is normal to the cut surface (Figure 8) and the direction of the main cutting force is given by the cutting velocity. Therefore, the global cutting force is given by the combination of the these two forces.

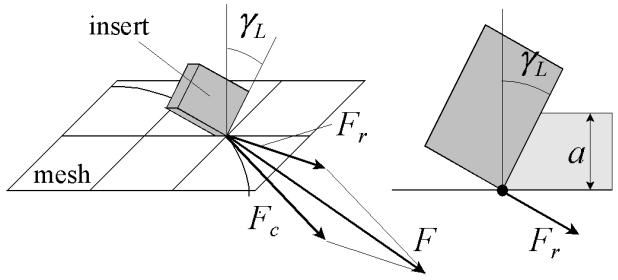

Figure 8: Cutting force direction

The directional coefficient u is given by

$$u = \cos\alpha\cos(\alpha-\beta) = (\boldsymbol{v_1}\cdot\boldsymbol{u_h})(\boldsymbol{v_1}\cdot\boldsymbol{u_f}) \tag{12}$$

where $\boldsymbol{v_1}$ is the greatest flexibility direction, $\boldsymbol{u_h}$ is the direction normal to the cut surface and $\boldsymbol{u_f}$ is the direction of the cutting force. Vectors $\boldsymbol{u_h}$ and $\boldsymbol{u_f}$ depend on the tool trajectory, the cutter diameter and the lead angle.

3.3 Discussion

The aim of chatter maps is to give process engineers a quick way to test and to improve a process setup. For the rough milling operation of the crankcase top deck presented in the following Section, the time to obtain the chatter map is about 40 minutes on a standard PC. Moreover, several parameters such as mill geometry or tool trajectory may be tested *interactively* since the flexibility map is already computed. It is also possible to quickly improve the fixture design in order to reduce chatter. Actually, each fixture design requires only the computation of a new flexibility map, which is obtained very rapidly since it requires only a new inversion of the reduced stiffness matrix (eq. 9). For the crankcase example, it takes about one minute.

It should be noticed that chatter maps will be used mainly in *process design phases*. At that time, the actual mass production part or a prototype may not yet exist. Thus, some model inputs (damping ratio and cutting stiffness) cannot be measured. Consequently, educated guess will determine the input values to compute the chatter map. With some experience, it should be possible to refine the model inputs, especially the damping ratio.

4 CASE STUDY

The case study presented concerns troubleshooting of the rough milling of a crankcase top deck on an existing high capacity transfer line. Workpiece geometry is shown in Figure 9.

Workpiece material is a grey cast iron. Rough face milling is performed using a ø400 mm cutter equipped with 64 ISO TN type inserts; the cutter axis moves along the longitudinal axis of the crankase. Nominal depth of cut for this operation is 3 mm, with a tolerance of ± 1.5 mm due to top deck position dispersion of the casting and previous machining operations (starting points of machining).

This operation has been affected by strong vibrations, resulting in a strong noise, a degrada-

tion of tool life and a consequent increase of tooling cost of up to 60 kEUR/year with respect to process design target. A close look at the machined surface reveals chatter marks on the external walls of the oil return (Figure 10).

Figure 9: Crankcase model.

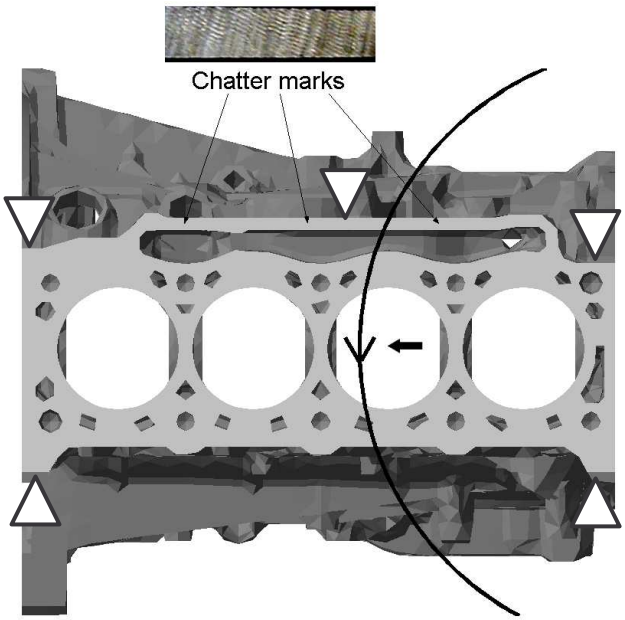

Figure 10: Cutter rotation direction, feed direction, and chatter marks. White triangles show clamping points.

Chatter vibrations are due to low stiffness of the thin external structure, despite the presence of a central stiffener in the clamping fixture. This is confirmed by comparison of the vibration spectrum obtained during the operation (Figure 11), chatter marks wavelength and the frequency response function of the clamped workpiece in the vibration area (Figure 12). During machining high vibrations levels are measured in the range 3000-4000 hertz and 5000-6000 hertz, depending on the cutter position; these frequency ranges correspond to the resonant frequency ranges of the thin walls, obtained by FRF measurements.

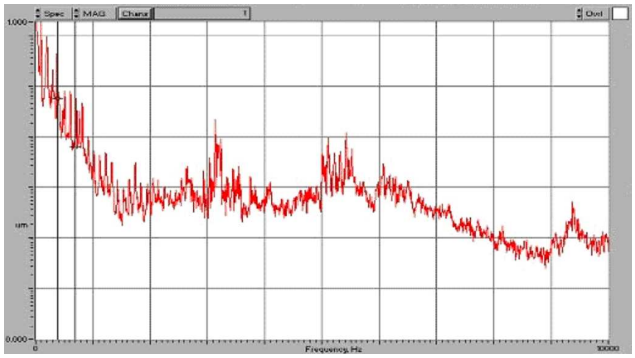

Figure 11: Frequency spectrum measured throughout the rough milling operation (cutting conditions S=92 RPM, F= 952 mm/min). Frequency axis (horizontal): 0-10000 Hz. Displacement amplitude (vertical, log scale): 10^{-6} to 1 µm. Accelerometer on clamping fixture.

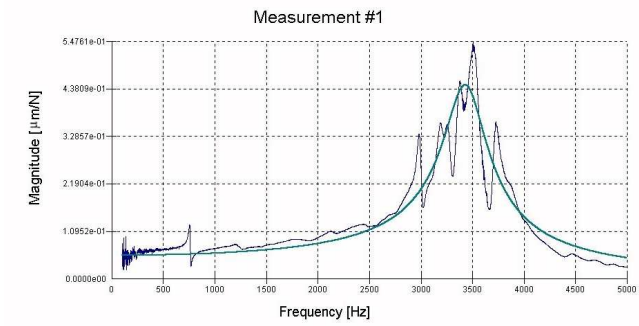

Figure 12: Magnitude of the TF for the oil return wall. Accelerometer oriented transversally to the thin wall on the chatter mark located on the right side in figure 10; excitation with an impact hammer, across the wall.

In this case the tooth passing frequency is 30 to 50 times smaller than the natural frequency of the structure. It is therefore impossible to select a spindle speed in order to operate within a stability lobe, since

i) the stability lobe would be extremely narrow;
ii) in mass production workpiece variability (i.e. minor changes in the natural frequency of the workpiece structure) would displace the stability lobe at every machined part.

A machining test, in which spindle speed was varied in the range 80-120 RPM, showed that

both vibration levels and frequencies in the thin walls were insensitive to spindle speed.

The chatter map obtained using the 6% damping coefficient obtained by modal analysis is shown in Figure 13. The three zones where chatter marks occur may be clearly identified. Maximum allowable depth of cut is 1.8 mm.

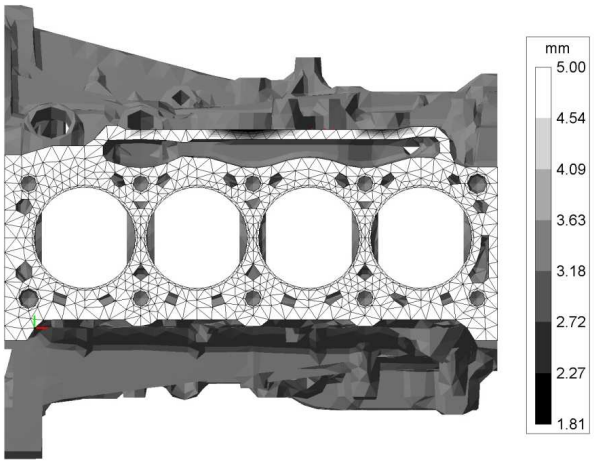

Figure 13: Chatter map for a 400mm cutter and a 45° lead angle.

Simulation results were confirmed experimentally by a machining test in which the oil return wall was pre-machined to give a controlled local depth of cut (1, 2 and 3 mm). The influence of the depth of cut on the vibration level is shown in Figure 14. A depth of cut of 1mm eliminates chatter whereas a tenfold increase of the vibration level is observed starting at a depth of cut of 2 mm.

In such a case, chatter could be eliminated effectively only if the operation took place below the unconditional stability limit. According to Tlusty's theory, effective countermeasures to obtain stable machining are achieved by

i) decreasing the cumulated cutting depth
ii) stiffening the structure
iii) lowering the specific feed force
iv) increasing the system's damping
orienting the feed force along the direction of maximum system's stiffness.

In the case of an existing mass production transfer machine, the freedom to implement such countermeasures is limited by technical and economical constraints. In particular, this example was characterized by a rather limited room for improvement. Stiffening the structure of the oil return wall would imply a weight increase, and a costly engine validation loop. Increasing system damping and changing the orientation of the feed force would demand considerable modification of the transfer machine. The depth of cut could not be decreased by a modification of the casting due to process capability and tolerance stack considerations. Reducing the number of cutting teeth would be useless because only one tooth at a time is engaged on the oil return wall.

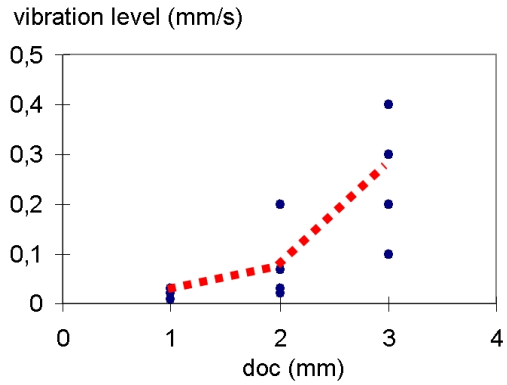

Figure 14: Peak vibration level in the range 2000-4000 Hz. Accelerometer on clamping fixture.

It was therefore decided to design a special *step cutter* [10] to reduce the nominal depth of cut in two equal parts by placing the cutting inserts on two diameters and distances from the spindle nose so that only one insert at a time would be cutting on the thin wall, with a nominal depth of cut of 1.5 mm at each step. Design constraints were also the minimum cutter diameter (400 mm, given by the total feed stroke) and maximum cutter diameter (430 mm at most to avoid collision with the clamping fixture). A 43+43 insert cutter was selected. Since the production unit does not allow a feedrate variation, a higher feed per tooth with respect to the previous 64 insert cutter is reached, with presumably beneficial effects in terms of proces damping. Before launching, in partnership with the tooling supplier, detailed design and production of the cutter and adapter plate, its design principle was validated by simulation. For the prototype step cutter, the lead angle for the two stages are respectively 53.8° and 60°. The maximum depth of cut obtained thanks to the chatter maps are 2.1 and 2.4 mm, considering a damping ratio of 6% as obtained by modal tests. Results obtained for a damping ratio varying from 3% to 6% are presented on Figure 15. The actual cutter is shown in Figure 16.

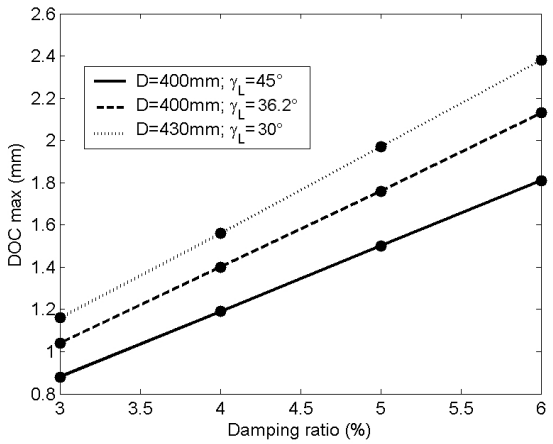

Figure 15: Evolution of maximum depth of cut at various damping ratios for the 45° lead angle cutter and the two-step cutter.

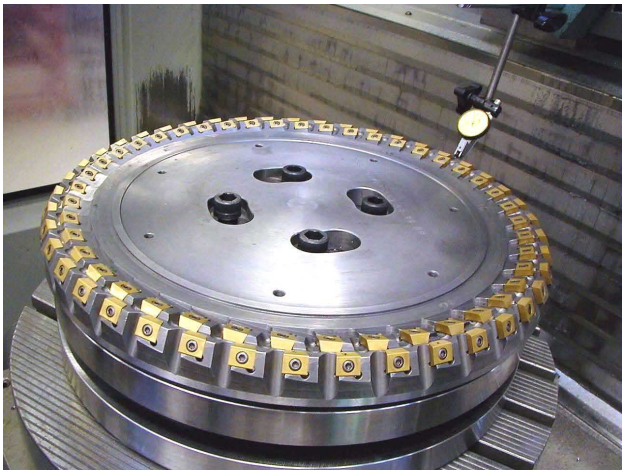

Figure 16: Two-step cutter

The prototype step cutter has been recently tested in an extensive field trial. Chatter disappeared, tool life had a threefold increase and noise levels of the post were lowered by more than 6 dB. The new cutter proved beneficial also in terms of a two-fold reduction of the deck face flatness after the operation.

5 CONCLUSION

This article describes a simulation model to compute a chatter map, which is used to identify the zones of the workpiece where chatter will occur. The approach is only valid for the thin walls of the workpiece. Nevertheless, chatter will mostly occur on these flexible structures. The model was applied to sudy the industrial case of a rough milling operation on a crankcase deck. Chatter maps were confirmed by machining tests, and results were used to design a special step cutter. The simulation model proposed in this article has been used as an effective decision support system for robust process design. In the future, this methodology can be increasingly used at the early stages of concurrent product-process design loops.

6 ACKNOWLEDGEMENT

We are grateful to Sandvik Coromant France for their support in carrying out the detailed design and production of the tooling.

7 REFERENCES

[1] H. Schulz, K. Bimschas, 1993, Optimization of precision machining by simulation of the cutting process, CIRP Annals, 42/1:55-59.

[2] D. A. Stephenson, 2002, Casting and machining process analysis at GM powertrain, S.A.E. technical paper 2002-01-0622:1-12.

[3] Q. Liu, C. Zhang, H.-P. Ben Wang, 1997, Form-accuracy and predction in computer integrated manufacturing, Int. J. Mach. Tools Manufact., 37/3: 237-248.

[4] N.N. Kakade, J.G. Chow, 1993, Finite element analysis of engine bore distortions during boring operation, ASME Trans. Journal of Engineering for Industry, 115:379-384.

[5] G. Subramani, M.C. Whitmore, S.G. Kapoor and R.E. DeVor, 1991, Temperature distribution in a hollow cylindrical workpiece during machining: theoretic model and experimental results, ASME Trans. Journal of Engineering for Industry, 113/4:373-380.

[6] L. Masset, 2001, Simulation of Face Milling and Turning with the Finite Element Method, International Journal of Forming Processes, 4/3-4:481-498.

[7] L. Masset, J.-F. Debongnie, P. Beckers, 2001, Face Milling and Turning simulation with the Finite Element Method, Proc. of the Fourth International ESAFORM Conference on Metal Forming, 627-630.

[8] Y Altintas, 2004, Dynamic cutting, CIRP Annals 53/2 (to be published).

[9] G. Tlusty, 1999, Manufacturing Processes and Equipment, Prentice hall.

[10] W. Belluco, 2003, Procédé d'usinage d'une face de carter et outil pour la mise en oeuver d'un tel procédé, patent request 03 12 014, request date 09.29.2003, INPI, France.